Effect of Li$^+$-ion on enhancement of photoluminescence in Gd$_2$O$_3$:Eu^{3+} nanophosphors prepared by combustion technique

N. Dhananjaya [a,b], H. Nagabhushana [c,*], B.M. Nagabhushana [d], B. Rudraswamy [a], C. Shivakumara [e], R.P.S. Chakradhar [f,*,1]

[a] Department of Physics, J.B. Campus, Bangalore University, Bangalore 560 056, India
[b] Department of Physics, B.M.S. Institute of Technology, Bangalore 560 064, India
[c] Department of PG studies & Research in Physics, University Science College, Tumkur University, Tumkur 572 103, India
[d] Department of Chemistry, M.S. Ramaiah Institute of Technology, Bangalore 560 054, India
[e] Solid State and Structural Chemistry Unit, Indian Institute of Science, Bangalore 560 012, India
[f] Central Glass and Ceramic Research Institute (CSIR), Kolkata 700 031, India

ARTICLE INFO

ABSTRACT

Gd$_2$O$_3$:Eu^{3+} (4 mol%) nanophosphor co-doped with Li$^+$ ions have been synthesized by low-temperature solution combustion technique in a short time. Powder X-ray diffractometer (PXRD), scanning electron microscopy (SEM), Fourier transform infrared spectroscopy (FT-IR), UV–VIS and photoluminescence (PL) techniques have been employed to characterize the synthesized nanoparticles. It is found that the lattice of Gd$_2$O$_3$:Eu^{3+} phosphor transforms from monoclinic to cubic as the Li$^+$-ions are doped. Upon 254 nm excitation, the phosphor showed characteristic luminescence $^5D_0 \rightarrow {}^7F_J$ ($J = 0$–4) of the Eu^{3+} ions. The electronic transition located at 626 nm ($^5D_0 \rightarrow {}^7F_2$) of Eu^{3+} ions was stronger than the magnetic dipole transition located at 595 nm ($^5D_0 \rightarrow {}^7F_1$). Furthermore, the effects of the Li$^+$ co-doping as well as calcinations temperature on the PL properties have been studied. The results show that incorporation of Li$^+$ ions in Gd$_2$O$_3$:Eu^{3+} lattice could induce a remarkable improvement of their PL intensity. The emission intensity was observed to be enhanced four times than that of with out Li$^+$-doped Gd$_2$O$_3$:Eu^{3+}.

© 2010 Elsevier B.V. All rights reserved.

1. Introduction

Nowadays, phosphors with high performances such as sufficient brightness, fast response and long term stability are required for the progress of modern luminescence devices [1]. The rare earth activated oxide phosphors have good luminescent characteristics, stability in high vacuum, and absence of corrosive gas emission under electron bombardent when compared to currently used sulfide based phosphors. The red-emitting phosphors doped with trivalent rare-earth (RE) ions have been widely used in the development of emissive display and tricolor lamp industry for two decades. In the past, Li$^+$ ion has been introduced in to different oxide hosts such as Y$_2$O$_3$:Eu^{3+} [2], Gd$_2$O$_3$:Eu^{3+} [3], SnO$_2$:Eu^{3+} [4], acting as a co-activator and charge compensator. It has been found that the PL intensity was substantially enhanced after Li$^+$ doping. It has

recently been reported that Li$^+$ site could result in the enhancement of up conversion emission in Gd$_2$O$_3$:Eu^{3+} [5]. It indicates that the improved up-conversion intensity may originate from the break of local crystal field symmetry around rare-earth ions by the Li$^+$ doping. Since Li$^+$ ion is very small, it can easily enter the host lattice, occupying not only the substitutional sites but also the interstitial sites [6]. Both the substitutional Gd^{3+} ions and the occupation of interstitial sites can break the symmetry of the crystal field around the rare-earth ions and the break can enhance the PL intensity.

The Li$^+$ ions, even in very small quantities as the dopant, frequently play an important role in increasing the luminescent efficiency of phosphors. Therefore, alkali metal ions such as Li$^+$, Na$^+$, K$^+$ were used to modify the local site symmetry of Eu^{3+} for improving the luminescence efficiency, owing to their chemical nature of low oxidation states and distinct ionic radii. A number of methods such as combustion [7], solid state [5], sol–gel [8] were employed to fabricate the Gd$_2$O$_3$:Eu^{3+} nanoparticles. Among, these methods, solution combustion technique is more attractive owing to the advantages of the simple equipment, low process temperature, time consumption, high purity and easily controlled particle size.

* Corresponding authors.
   E-mail addresses: bhushanvl@rediffmail.com (H. Nagabhushana), sreechakra72@yahoo.com, chakra72@gmail.com (R.P.S. Chakradhar).
[1] Present address: Scientist, CSIR-NAL, Bangalore 560 017, India.

To the best of our knowledge, the systematic studies on Li$^+$ co-doping on the structural and PL studies of Gd$_2$O$_3$:Eu^{3+} is very limited. As a part of our programme on phosphor materials [9–12], here we report, the effect of Li$^+$-ion on structural and enhancement of photoluminescence properties of Gd$_2$O$_3$:Eu^{3+} nanophosphors prepared by combustion technique. It is generally regarded that the luminescent efficiency of phosphor is reduced with the decrease of the grain size due to a large contribution of the surface states to the non-radiative transition [13]. On the other hand, a change in the composition of phosphor, such as the incorporation of Li$^+$ ion into host material, is an effective way to enhance its luminescent performance. The role of the Li$^+$ ion is mainly attributed to the flux effect and the creation of oxygen vacancy [14]. Therefore, it is expected that the luminescent efficiency will be improved further by co-doping with several dopants.

2. Experimental

2.1. Synthesis of Li$^+$-doped Gd$_2$O$_3$:Eu^{3+} nanoposphors

The starting chemicals used for the preparation of Gd$_2$O$_3$:Eu^{3+} (Li$^+$) nanophosphors were of analar grade gadolinium nitrate [Gd(NO$_3$)$_3$], europium nitrate [Eu(NO$_3$)$_3$] and lithium nitrate [LiNO$_3$]. The oxalyl dihydrazide [ODH: C$_2$H$_6$N$_4$O$_2$] is used as a fuel for combustion synthesis and was prepared in our laboratory [15]. An aqueous solution containing stoichiometric amounts of gadolinium nitrate, europium nitrate, lithium nitrate and ODH have been taken in a cylindrical Petri dish of ~300 ml capacity. The excess water is allowed to evaporate by heating over a hot plate until a wet powder is left out. Then the Petri dish is introduced into a muffle furnace maintained at 400 ± 10 °C. The reaction mixture undergoes thermal dehydration and ignites at one spot with liberation of gaseous products such as oxides of nitrogen and carbon. The combustion of ODH is exothermic and releases the energy required for the synthesis. The combustion propagates throughout the reaction mixture without further need of any external heating, as the heat of reaction is sufficient for the decomposition of redox mixture. The flame temperature was found to be 1000 ± 50 °C, which persists for few seconds, and was measured by an optical pyrometer placed inside the muffle furnace. The flow chart for the synthesis Gd$_2$O$_3$:Eu^{3+} (Li$^+$) phosphor is given in Fig. 1.

2.2. Instruments used

The phase purity of the nanophosphors is examined by powder X-ray diffractometer (PXRD) (PANalytical X'Pert Pro) using CuK$_\alpha$ radiation with a nickel filter was used to estimate the crystallinity of the phases. The surface morphology of the product is examined by Scanning Electron Microscopy (SEM) (JEOL JSM 840A) by sputtering technique with gold as covering contrast material. The FT-IR studies have been performed on a Perkin Elmer Spectrometer (Spectrum 1000) with KBr pellets. The UV–VIS absorption of the samples was recorded on SL 159 ELICO UV–VIS Spectrophotometer. The photoluminescence (PL) measurements were performed on a Shimadzu Spectroflourimeter (Model RF 510) equipped with 150 W Xenon lamp as an excitation source.

3. Results and discussion

Fig. 2(a) shows the powder X-ray diffraction patterns of Gd$_2$O$_3$:Eu^{3+}:Li$^+$ (0–8 mol%) phosphors calcined at 800 °C for 3 h. The Gd$_2$O$_3$:Eu^{3+} nanopowders indexed to mixed phase of monoclinic (JCPDS no. 43-1015) and cubic (JCPDS no. 86-2477) structure respectively. The sharp and intense peaks clearly show the crystalline nature of the sample. As Li$^+$ concentration increases the mixed phase becomes more likely to be cubic phase. The ratio of the peak values $I_C(2\,2\,2)/I_M(4\,0\,2)$ (Intensity of cubic phase to monoclinic phase) increased from 1.17 to 4.79. The crystallite size was calculated from the broad PXRD peaks using the Scherer's equation [16]
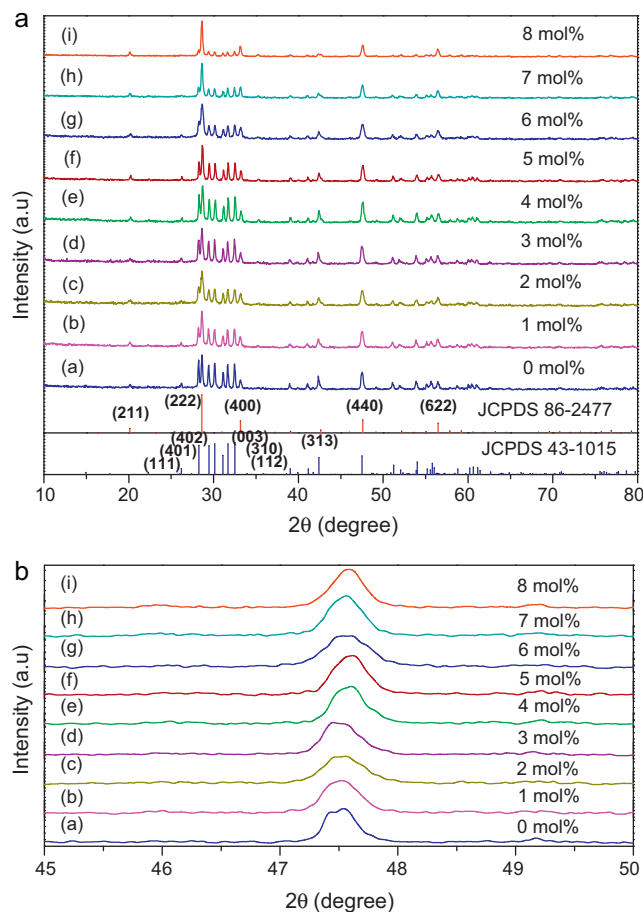
$$d = \frac{0.9\lambda}{\beta \cos \theta} \tag{1}$$

Fig. 1. Flow chart for the synthesis of Gd$_2$O$_3$:Eu^{3+}(Li$^+$) nanophosphor.

Fig. 2. (a) PXRD patterns of Gd$_2$O$_3$:Eu^{3+}:Li$^+$ (0–8 mol%) nanophosphors calcined at 800 °C for 3 h. (b) PXRD patterns of Gd$_2$O$_3$:Eu^{3+}:Li$^+$ (0–8 mol%) nanophosphors (at 2θ = 47.5 (4 4 0)) calcined at 800 °C for 3 h.

Table 1
Parameters calculated with respect various Li$^+$ ion concentrations.

Sample	FWHM (degree) $2\theta = 28.68°$	Grain size(nm)		Band gap (eV)
		Scherer's method (d)	W–H method (D)	
Gd$_2$O$_3$:Eu^{3+}	0.3552	25.51	29.28	4.47
Gd$_2$O$_3$:Eu^{3+}:Li(1 mol%)	0.3357	26.99	31.73	4.83
Gd$_2$O$_3$:Eu^{3+}:Li (2 mol%)	0.2560	35.39	40.88	5.43
Gd$_2$O$_3$:Eu^{3+}:Li (3 mol%)	0.2495	36.32	42.95	5.41
Gd$_2$O$_3$:Eu^{3+}:Li (4 mol%)	0.2480	36.65	45.95	5.42
Gd$_2$O$_3$:Eu^{3+}:Li (5 mol%)	0.2402	37.73	48.23	5.23
Gd$_2$O$_3$:Eu^{3+}:Li (6 mol%)	0.2210	41.01	51.32	5.16
Gd$_2$O$_3$:Eu^{3+}:Li (7 mol%)	0.2092	43.32	52.32	4.81
Gd$_2$O$_3$:Eu^{3+}:Li (8 mol%)	0.2005	45.19	54.19	4.60

where d is the average grain size of the crystallites, λ the incident wavelength, θ the Bragg angle and β the diffracted full-width at half-maximum (FWHM) in radians caused by the crystallites. The mean crystallite size calculated from this method is found to be in the range 25–45 nm.

The grain size was also calculated from the powder X-ray diffraction line broadening (B) using the analysis described by Williamson and Hall (W–H) method [17].

$$B \cos\theta = \varepsilon(4 \sin\theta) + \frac{\lambda}{D} \qquad (2)$$

where B (FWHM in radian) is measured for different XRD lines corresponding to different planes, ε is the strain developed and D is the grain size. The equation represents a straight line between $4\sin\theta$ (X-axis) and $B\cos\theta$ (Y-axis). The slope of line gives the strain (ε) and intercept (λ/D) of this line on the Y-axis gives grain size (D).

The grain size determined from W–H formula is slightly higher than those calculated using Scherrer's formula (Table 1). The small variation in the values is due to the fact that in Scherrer's formula strain component is assumed to be zero and observed broadening of diffraction peak is considered as a result of reducing grain size only. Strain continues to increase with an increase in Li$^+$ concentration. These results indicated that the host lattice dimension shrinks with the concentration of Li$^+$ from 0 mol% and then begins to expand when the concentration of Li$^+$ is over 5 mol%. The effective ionic radius of Gd^{3+} ion and Li$^+$ ion are 0.94 Å and 0.76 Å respectively [18]. Hence, substitutes the Gd^{3+} ion with these smaller Li$^+$ ion can induce the shrinking of the host lattice, whereas Li$^+$ ions occupying the interstitial sites leads to the expansion of the host lattice consequently, when the concentration of Li$^+$ ions is below 5 mol%, Li$^+$ ions occupy substitutional sites, but with higher concentrations, Li$^+$ ions begin to take interstitial sites. The both types of Li$^+$ occupancies would break the local crystal field symmetry around the Eu^{3+} ions, Li$^+$ ions doping could help to break the forbidden transition, change the life time of energy levels and consequently enhance the intensity. As Li$^+$ content was increased from 0 to 4 mol% crystallinity improved. However, when Li$^+$ content was increased, further to 5 mol%, the crystallinity decreases, this result may be induced by increase of oxygen vacancies by Li$^+$ ion substitution [19]. These oxygen vacancies in lattice weakened bond strength such that the lattice constant increased [20]. The lattice parameters to be observed shifted towards larger values due to lattice expansion with increase in Li$^+$ concentration. Occupation of Li$^+$ ion would naturally give rise to a substantial number of vacant sites in oxygen ion and then expand the lattice with decrease of crystal density. So the lattice expansion can be attributed to the weakening of bond strength due to the formation of oxygen vacancies [21]. Better crystallization and larger grain size can be regarded as the result of the Li$^+$ ions during the preparation process, which plays an important role in effectively promoting an incorporation of Eu^{3+} and Gd$_2$O$_3$ as well as Li$^+$ ions themselves in to the host lattice.

Fig. 2(b) shows the shift of the peak towards higher glancing angle, it is due to smaller size of Li$^+$ ion and it is conforms the incorporation of Li$^+$ ions in Gd$_2$O$_3$:Eu^{3+} lattice.

Fig. 3(a–e) shows the PXRD patterns of Li$^+$ (4 mol%) co-doped Gd$_2$O$_3$:Eu^{3+} samples calcined at 500, 600, 700, 800 and 900 °C for 3 h. It is observed that the intensity of the PXRD peaks increases with calcination temperatures. It is noticed that the ratio of peak values, $I_C(2\,2\,2)/I_M(1\,1\,1)$, increased from 0.79 to 1.48 with increase in calcination temperature 500–700 °C, and thereafter it start decreasing from 1.48 to 0.93 with further increase in calcinations temperature 800–900 °C.

Fig. 4 show the SEM photographs of without and with Li$^+$ (6 mol%) co-doped Gd$_2$O$_3$:Eu^{3+} phosphor. The un-doped phosphors are agglomerated from few microns to a few tens of microns, fluffy and porous in nature. The agglomeration of nanoparticles is usually explained as a common way to minimize their surface free energy. The voids and pores present in the sample are due to the large amount of gases produced during combustion synthesis. In Li$^+$ (6 mol%) doped Gd$_2$O$_3$:Eu^{3+} phosphor, the agglomeration is reduced and particles are in spherical in shape.

Fourier transform infrared spectral studies (Fig. 5) have been carried out on all Li$^+$-doped Gd$_2$O$_3$:Eu^{3+} samples. It is found that, the peaks around 400 and 540 cm^{-1} confirms the Gd–O peak. No other peak is noticed, this conforms the purity of the compounds.

The excitation spectra of without and with Li$^+$ (6 mol%) doping of Gd$_2$O$_3$:Eu^{3+} phosphors are illustrated in the Fig. 6(a and b) respectively. The peak near 250 nm in the excitation spectrum is known as the charge transfer (CT) peak which attributes to the transition
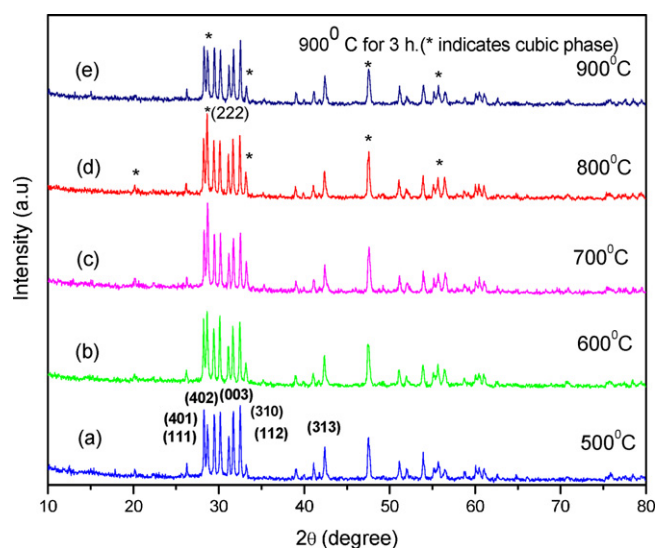
Fig. 3. PXRD patterns of Gd$_2$O$_3$:Eu^{3+}:Li$^+$ (4 mol%) phosphors calcined at (a) 500 °C, (b) 600 °C, (c) 700 °C, (d) 800 °C and (e) 900 °C for 3 h.
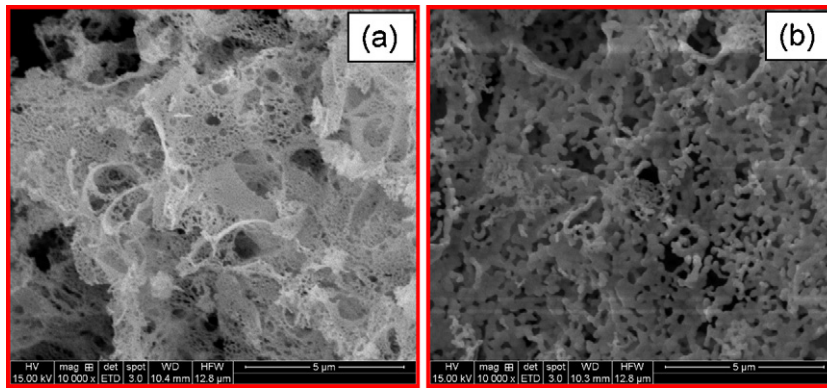
Fig. 4. SEM micrographs of nanophosphors calcined at 800 °C for 3 h (a) Gd_2O_3:Eu^{3+} and (b) Gd_2O_3:Eu^{3+}:Li^+ (6 mol%).
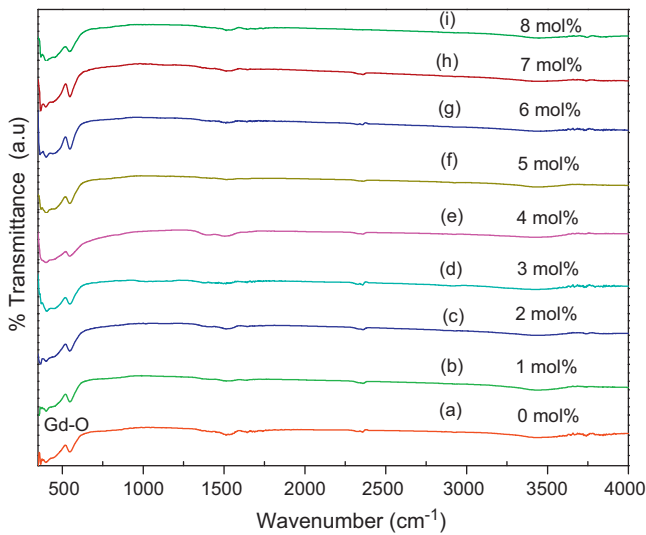

Fig. 5. FT-IR spectra of Gd_2O_3:Eu^{3+}:Li^+ (0–8 mol%) phosphors calcined at 800 °C (3 h).
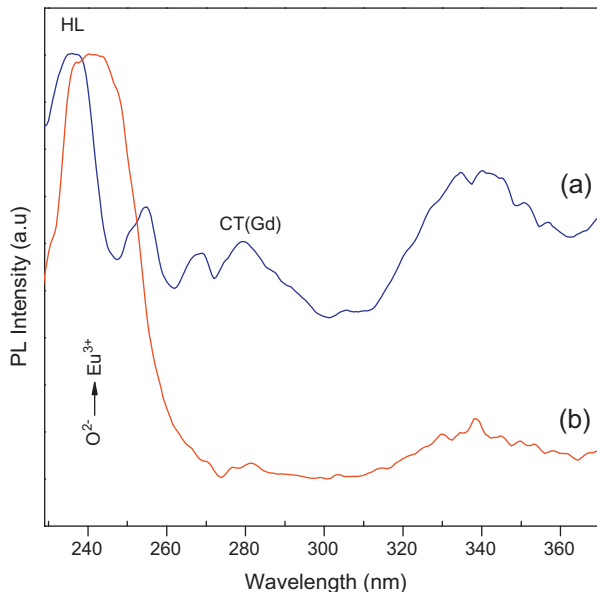
from O^{2-} 2p state to Eu^{3+} 4f state [18]. The peak near 240 nm originates from the excitation of Gd_2O_3 host lattice (HL). The HL and CT peak of the doped samples were improved distinctly in comparison with that of un-doped sample. It is noticeable that CT peak was almost unchanged in Li^+-doped samples. Lopez et al. [22] reported that the oxygen vacancy might act as a sensitizer for the energy transfer to the rare-earth ions owing to the strong mixing of CT states. Hence the second aspect can be ascribed to the creation of oxygen vacancies due to Gd^{3+} sites occupied by smaller Li^+ ions, resulting in the improvement of luminescent intensity.

It is observed that the host lattice peak in Li^+ co-doped Gd_2O_3:Eu^{3+} is shifted (~10 nm) towards higher wavelength side when compared to un-doped Li^+. In emission spectrum ($\lambda_{exi} = 254$ nm) (Fig. 7), the strongest peak situated at 612 nm is assigned to the $^5D_0 \rightarrow {}^7F_2$ transition of Eu^{3+} ions, and the peak around 588 nm is related to $^5D_0 \rightarrow {}^7F_1$ transition. The peaks from $^5D_1 \rightarrow {}^7F_J$ ($J = 1, 2$) transitions were also detected in the range of 525–570 nm. It is obvious that the PL intensity of Gd_2O_3:Eu^{3+} nanophosphor can be enhanced drastically by co-doping with Li^+ ions. Comparing with the un-doped samples, the PL intensities are improved 4 times for Li^+ co-doped Gd_2O_3:Eu^{3+} nanophosphors. The influence of the Li^+ ions on the luminescent performance may be attributed to several aspects. Firstly and the most obvious one is the flux effect of the Li^+. It gives a better crystallization and larger grain size, resulting in higher oscillating strengths for the optical transitions [23], and also reducing the luminescence quenching due to the surface states [13], thus bringing on the increase of the luminescent intensity. In addition, Li^+ ions promote the structured transforma-
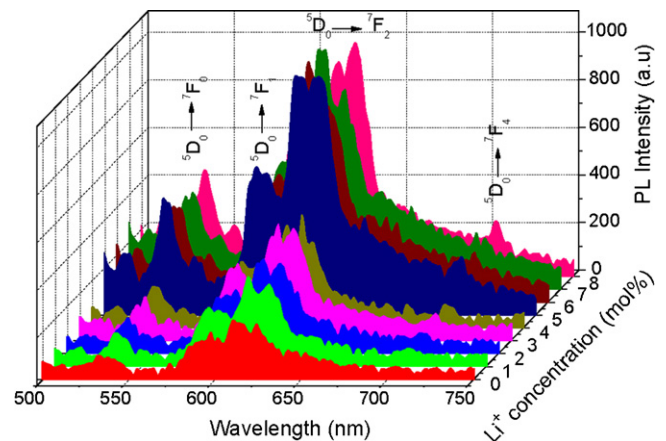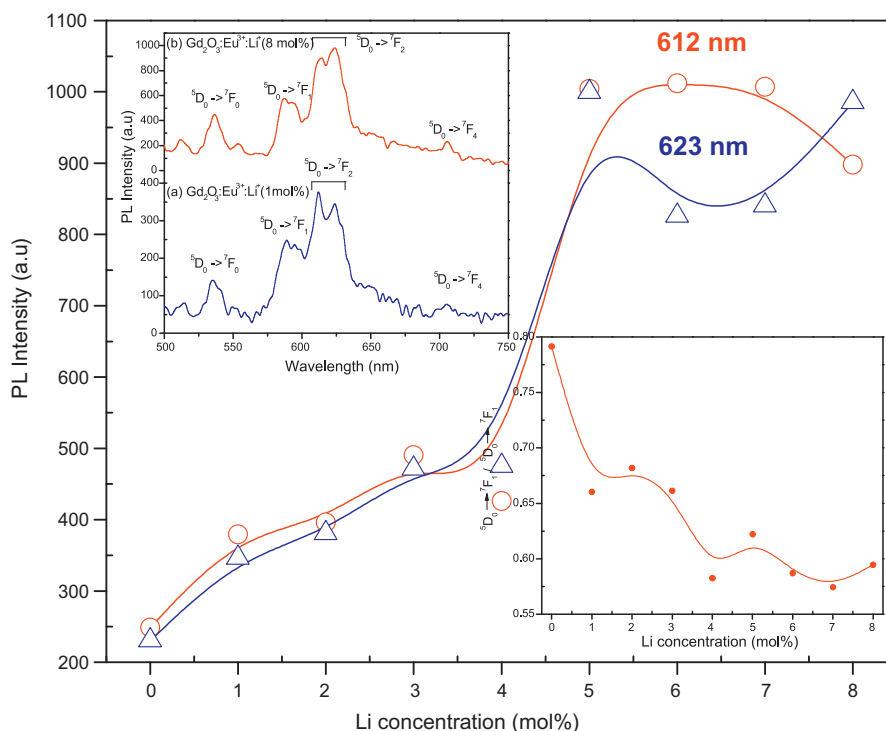

Fig. 6. Excitation spectra of (a) Gd_2O_3:Eu^{3+} and (b) Gd_2O_3:Eu^{3+}:Li^+ (6 mol%).

Fig. 7. PL emission spectra of Gd_2O_3:Eu^{3+}:Li^+ (0–8 mol%) nanophosphors calcined at 800 °C for 3 h.

Fig. 8. The variation of PL intensity as a function of Li$^+$ (0–8 mol%) content in Gd$_2$O$_3$:Eu^{3+} matrix. Inset: (i) PL comparison of Li$^+$ (1 and 8 mol%)of Gd$_2$O$_3$:Eu^{3+} nanophosphor. (ii) The variation of 612/623 peaks ($^5D_0 \rightarrow {}^7F_1/{}^5D_0 \rightarrow {}^7F_2$) as a function of Li$^+$ concentrations.

tion from monoclinic to cubic Gd$_2$O$_3$:Eu^{3+}. This structural change is favorable for luminescence. The effective ionic radius of Li$^+$ (0.76 Å) ion is smaller than that of Gd^{3+} ion (0.94 Å) and therefore the Li$^+$ ions are suitable for occupation of the Gd^{3+} sites, which will give rise to a number of oxygen vacancies for the charge neutrality.

When the concentration of Li$^+$ ion is below 4 mol%, substituting Gd^{3+} ions with Li$^+$ ions can induced oxygen vacancy due to charge compensation, so the substitutional site Li$^+$ ions and oxygen vacancies around Eu^{3+} ions can cause the crystal field distortion. However, for higher concentration of Li$^+$ the substitutional site and the interstitial site Li$^+$ ions co-exist in the host. These interstitial Li$^+$ ions would induce the Gd^{3+} vacancies so there are four different types of defects around the Eu^{3+} ions, which cause much severe crystal field distortion. When the content of Li$^+$ is above 4 mol%, the increase of emission peaks that stark levels have been split, which proves that with the appearance of interstitial Li$^+$ the crystal field symmetry around Eu^{3+} have been seriously broken.

Fig. 8 shows the PL intensity of the $^5D_0 \rightarrow {}^7F_1$ (612 nm) and $^5D_0 \rightarrow {}^7F_2$ (623 nm) transition of the Gd$_2$O$_3$:Eu^{3+} (4 mol%) nanophosphor as a function of Li$^+$ (0–8 mol%) doping concentration. It can be seen that the intensities of the $^5D_0 \rightarrow {}^7F_2$ transitions are always higher than that of the $^5D_0 \rightarrow {}^7F_1$ transitions irrespective of the Li$^+$ concentration. The emission intensity resulting from the $^5D_0 \rightarrow {}^7F_1$ and $^5D_0 \rightarrow {}^7F_2$ transitions are prominently enhanced after substitution of (4 mol%) Eu^{3+} by Li$^+$ and the emission intensity further increases with the Li$^+$ concentration obtaining its maximum at 6 mol% Li$^+$, then slightly decrease. This phenomenon is probably due to the fact that low fraction of Li$^+$ substitution in the lattice induce the fast energy transfer from the host to the Eu^{3+} ions and a decrease in interstitial oxygen, and hence conducting an increase in the hole concentration leading to a decrease in competitive absorption and as a result to a higher quantum yield [24]. On the other hand the doping of Li$^+$ might also give rise to the formation of defective structure. Once Li$^+$ attains a certain concentration (5, 6 and 7 mol%), the defects in the host lattice greatly increase, which would unavoidably reduce the crystallinity and increase

the unactive center concentration, thus leads to the luminescence quenching [25].

Therefore, the PL intensity has great dependence on co-activator concentration. The brightness increases with co-activator concentration to certain extent, if above this point, the luminescence begins to decrease, due to parity or aggregation of co-activator atoms at high concentration which leads to efficient resonant energy transfer between Eu^{3+}/Li$^+$ ions and a fraction of energy migration to distant killer or quenchers, then quenching behavior appears as a result.

The PL intensity ratios of the $^5D_0 \rightarrow {}^7F_1$ transition to the $^5D_0 \rightarrow {}^7F_2$ transitions at various Li$^+$ concentrations are shown in inset of Fig. 8. It is well known that the $^5D_0 \rightarrow {}^7F_2$ transition is allowed when Eu^{3+} embedded at a site of non-inversion symmetry while $^5D_0 \rightarrow {}^7F_1$ transition is allowed at a site with inversion symmetry. Hence, the PL intensity ratio $^5D_0 \rightarrow {}^7F_1/{}^5D_0 \rightarrow {}^7F_2$ called as symmetric ratio, gives a measure of the degree of distortion from inversion symmetry of the local environment surrounding the Eu^{3+} ions in the host matrix [26]. However, it is reasonable to believe that the doping of Li$^+$ will introduce lattice defects, which will undoubtedly reduce the symmetry strength of the local environment of Eu^{3+}. Consequently, the symmetry ratio of Gd$_2$O$_3$:Eu^{3+}:Li$^+$ decreases with the increase of doped Li$^+$ concentration (inset Fig. 8).

Fig. 9(a–e) shows the Gd$_2$O$_3$:Eu^{3+}:Li$^+$ (4 mol%) nanophosphor heat treated at different temperatures from 500–900 °C. The PL intensity of $^5D_0 \rightarrow {}^7F_1$ and $^5D_0 \rightarrow {}^7F_2$ transition plotted as a function of calcinations temperature is shown in Fig. 10. It is observed that, PL intensity increases with increase of calcinations temperature. The crystal structure of the sample observed at low-temperature is faintly disorder and quenching centers, resulting in better emission. However, when temperature is raised over the certain point, this effect becomes less prominent and as a result the emission intensity reaches its saturations. For the enhanced PL intensity, it can be suggested that the incorporation of Li$^+$ ions creates the oxygen vacancies, which might act as a sensitizer for the effective energy transfer due to the strong mixture of charge transfer states [18].
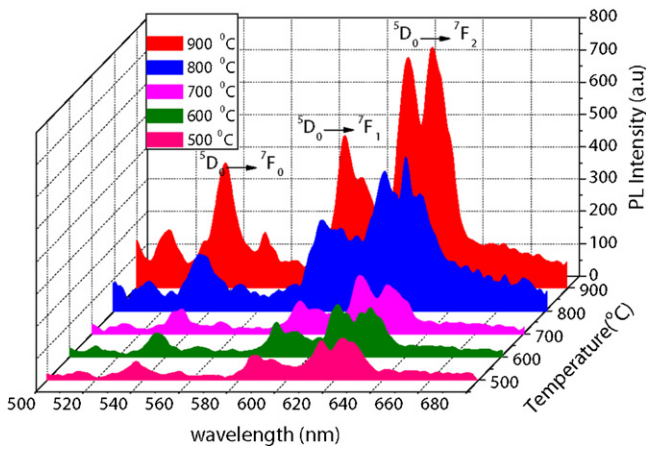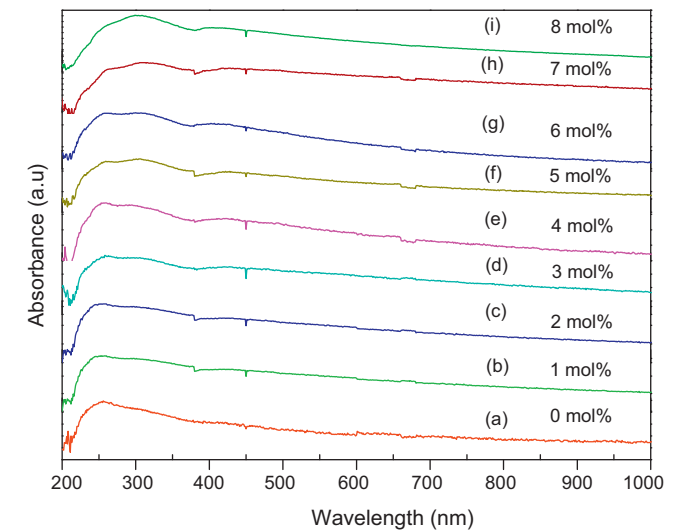
Fig. 9. PL emission spectra of Gd_2O_3:Eu^{3+}:Li^+ (4 mol%) nanophosphors calcined at different temperature for 3 h.

Fig. 11. UV–VIS spectra of Gd_2O_3:Eu^{3+}:Li^+ (0–8 mol%) phosphors calcined at 800 °C (3 h).

The UV–VIS absorption spectra of Li^+ (0–8 mol%) Gd_2O_3:Eu^{3+} are shown in Fig. 11. Both of the spectra have strong absorption in the UV spectral region and some were peaks of intra- 4f transitions of Eu^{3+} at lower wavelength. The Li^+-doped sample exhibits a visible increase of absorbance and an obvious red-shift of the absorption edge compared with the one without Li^+ doping. It has been known that the position of the absorption edge is determined by the width of forbidden band with O 2p orbits as the valence band in multi component oxides. Occupation of Gd^{3+} sites by Li^+ ions would naturally give rise to a substantial number of oxygen vacancies, which may change the energy band structure and enhance the deformation degree of O 2p orbits and the superposition of the electronic wave functions, and then result in narrowing the forbidden band and shifting the absorption edge to the red.

The optical band gap energy (E_g) (Fig. 12) was estimated by the method proposed by Tauc [27]. According to these authors, the optical band gap is estimated with absorption co-efficient and photon energy by the following equation

$$h\nu\alpha \propto (h\nu - E_g)^k \qquad (3)$$

where α is the absorption co-efficient, h is the Planks constant, ν is the frequency, E_g is the optical band gap and k is the constant associated to the different types of electronic transitions $k = 1/2$,

2, 3/2, 3 for direct allowed, indirect allowed, direct forbidden and indirect forbidden transitions respectively. According to literature [28] the oxides are characterized by an indirect allowed electronic transition and hence, the $k = 2$ value was adopted as standard in Eq. (3). Thus the E_g values was evaluated extrapolating the linear portion of the curve or tail [$(h\nu\alpha)^{1/k} = 0$] in the UV–VIS absorbance spectra. A plausible explanation for the variations observed in the E_g values can be related to the degree of structural order–disorder in to the lattice, which is able to change the intermediary energy level distribution within the band gap. The variations in the band gap values might also be due to higher degree of structural defects, while the phosphors heat treated from 500 to 900 °C, the absorption spectra shows more ordered/crystalline materials (inset Fig. 13). On the basis of these information, if the structure becomes more ordered with the heat treated temperature i.e. when the concentration of structural defects (oxygen vacancies, distortions and/or strains in the lattice) is reduced. The presence of intermediary energy levels (deep and shallow holes) is minimized within the optical band gap and consequently, the E_g values increase. As it can be seen, the energy gap values (Table 1) are mainly depends on the
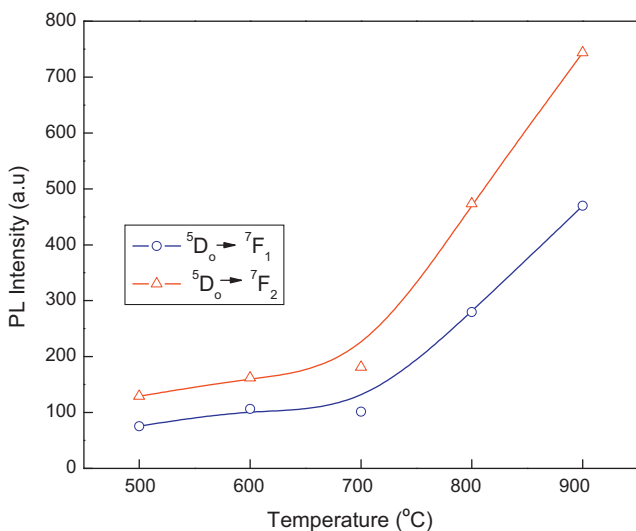
Fig. 10. The variation of PL intensity of $^5D_0 \rightarrow ^7F_1$ and $^5D_0 \rightarrow ^7F_2$ transition as a function of calcination temperature (3 h).
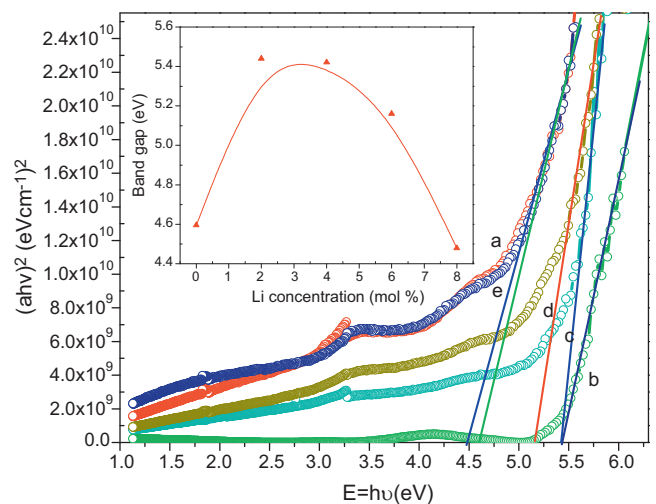
Fig. 12. Energy gap of Gd_2O_3:Eu^{3+}:Li^+ phosphors calcined at 800 °C (3 h) (a) without Li^+, (b) 2 mol%, (c) 4 mol%, (d) 6 mol% and (e) 8 mol% respectively (inset: band gap vs. Li^+ concentration).
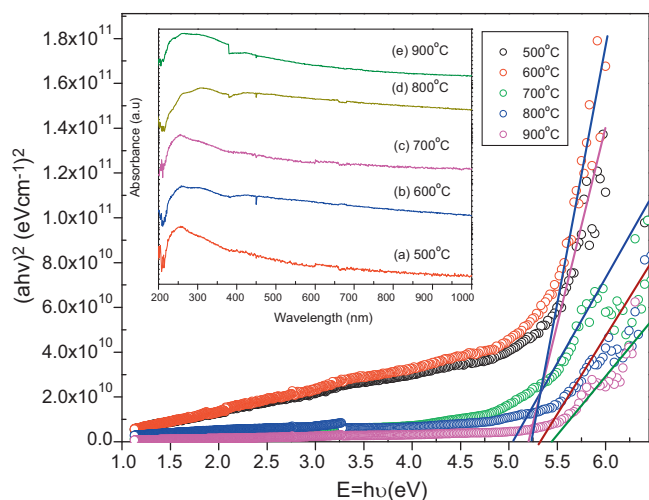
Fig. 13. Energy gap of Gd_2O_3:Eu^{3+}:Li^+ phosphors calcined at different temperature (a) 500 °C, (b) 600 °C, (c) 700 °C, (d) 800 °C and (e) 900 °C (inset: UV–VIS absorption spectra).

preparation methods and experimental conditions (heat-treated and processing time). In particular, these key factors can favor or inhibit the formation of structural defects, which are able to control the degree of structural order–disorder in the material and consequently, the number of intermediary energy levels within the band gap.

4. Conclusions

Li^+ co-doped (0–8 mol%) Gd_2O_3:Eu^{3+} red phosphors have been prepared through solution combustion synthesis. The improvement of the crystallinity and decrease of particle size induced by the addition of Li^+ ions has been observed. When Li^+ was co-doped, the PL intensity of Gd_2O_3:Eu^{3+} phosphor is enhanced. This is due to charge compensation resulting from the substitution effect of Li^+ ions to Gd^{3+} and also due to lowering of local symmetry that was induced by the Li^+ ions. The luminescence spectra consists of a dominant red emission peak at 612 nm, which corresponds to the transition of $^5D_0 \rightarrow {}^7F_2$ of Eu^{3+} ions. The higher PL emission intensity was observed in 6 mol% Li^+ whose brightness was increased by 4 times when compared to that of Gd_2O_3:Eu^{3+}. The improvement in the PL efficiency with the Li^+ doping may result from improved crystallinity leading to higher oscillating strengths for the optical transitions. Further, it can also be suggested that the incorporation of Li^+ creates the oxygen vacancies, which might act as a sensitizer for the effective energy transfer due to strong charge transfer states. Thus the red emitting Li^+-doped Gd_2O_3:Eu^{3+} phosphors are promising for possible display applications.

References

[1] J.H. Jeong, H. Koung Yang, B.K. Moon, J. Seong Bae, S.S. Yi, H.C.J. Hwan Kim, S.T. Chung, Opt. Mater. 28 (2006) 693.
[2] J.S. Bae, S.B. Kim, J.H. Jeong, J.C. Park, D.K. Kim, S.H. Byeon, S.S. Yi, Thin Solid Films 471 (2005) 224.
[3] T. Takeda, D. Koshiba, S. Kikkawa, J. Alloys Compd. 408 (2006) 879.
[4] D. Paul Joseph, P. Renugambal, M. Saravanan, S. Philip Raja, C. Venkateswaran, Thin Solid Films 517 (2009) 6129.
[5] S.H. Shin, J.H. Kang, D.Y. Jeon, D.S. Zang, J. Lumin. 114 (2005) 275.
[6] T. Dhannia, S.J Ayalekshmi, M.C. Santhosh Kumar, T Prasada Rao, A. Chandra Bose, J. Phys. Chem. Solids 71 (2010) 1020.
[7] L.D. Sun, C.S. Liao, C.H. Yan, J. Solid State Chem. 117 (2003) 304.
[8] R.P. Rao, Solid State Commun. 99 (1996) 439.
[9] R.P.S. Chakradhar, B.M. Nagabhushana, G.T. Chandrappa, J.L. Rao, J. Chem. Phys. 121 (2004) 10250.
[10] B. Umesh, B. Eraiah, B.M. Nagabhushana, H. Nagabhushana, H.B. Premkumar, C. Shivakumara, Chikkahanumantharayappa, R.P.S. Chakradhar, Phil. Mag. Lett. 89 (2009) 589.
[11] H. Nagabhushana, B.M. Nagabhushana, M. Kumar, H.B. Premkumar, C. Shivakumara, R.P.S. Chakradhar, Phil. Mag. 90 (2010) 3567.
[12] N. Dhananjaya, H. Nagabhushana, B.M. Nagabhushana, R.P.S. Chakradhar, C. Shivakumara, B. Rudraswamy, Physica B 405 (2010) 3795.
[13] H.S. Peng, H.W. Song, B.J. Chen, J.W. Wang, S.Z. Lu, X.G. Kong, J.H. Zhang, J. Chem. Phys. 118 (2003) 3277.
[14] X.D. Sun, X.D. Xiang, Appl. Phys. Lett. 72 (1998) 525.
[15] B.M. Nagabhushana, Combustion synthesis, characterization and study of magnetic properties of alkaline earth substituted lanthanum manganits, Ph.D. Thesis, Bangalore University, 2008.
[16] P. Klug, L.E Alexander, X-ray Diffraction Procedure, Wiley, New York, 1954.
[17] G.K. William, W.H. Hall, Acta Metall. 1 (1953) 22.
[18] B. Liu, M. Gu, X. Liu, C. Ni, D. Wang, L. Xiao, R. Zhang, J. Alloys Compds. 440 (2007) 341.
[19] Hongwu Zhang, Xiaoyan Fu, Shuyun Niu, Gongquan Sun, Qin Xin, J. Lumin. 115 (2005) 7.
[20] H.K. Yang, H. Choi, B.K. Moon, B.C. Choi, J.H. Jeong, J.H. Kim, K.H. Kim, Solid State Sci. 12 (2010) 1445.
[21] S.H. Shin, J.H. Kang, D.Y. Jeon, S.H. Choi, S.H. Lee, Y.C. You, D.S. Zang, Solid State Commun. 135 (2005) 30.
[22] O.A. Lopez, J. McKittrick, L.E. Shea, J. Lumin. 71 (1997) 1.
[23] K.C. Misbra, J.K. Berkowitz, K.H. Johnson, P.C. Schmidt, Phys. Rev. B 45 (1992) 10902.
[24] S.S. Yi, J.S. Bae, K.S. Shim, J.H. Jeong, J.C. Park, P.H. Holloway, Appl. Phys. Lett. 84 (2004) 353.
[25] X.L. Liu, X. Xui, M. Gu, L.H. Xiao, K. Han, R. Zhang, Appl. Surf. Sci. 253 (2007) 4344.
[26] G. Hebbink, J. Stouwdam, D. Reinhoudt, E. Beggel, Adv. Mater. 14 (2002) 1147.
[27] J. Tauc, in: F. Abeles (Ed.), Optical Properties of Solids, North-Holland, Amsterdam, 1970.
[28] X. Liu, F. Zhou, M. Gu, S. Huang, B. Liu, C. Ni, Opt. Mater. 31 (2008) 126.